INSTITUTE FOR NUCLEAR STUDY
UNIVERSITY OF TOKYO
Tanashi, Tokyo 188
Japan

INS-Rep.-588
June 1986

Photonuclear spallation reactions in Cu

S. SHIBATA, M. IMAMURA, T. MIYACHI, M. MUTOU
K. SAKAMOTO, Y. HAMAJIMA, M. SOTO, Y. KUBOTA,
M. YOSHIDA and I. FUJIWARA*

INS-Rep.-588
June 1986

Photonuclear spallation reactions in Cu

S. SHIBATA, M. IMAMURA, T. MIYACHI, and M. MUTOU

Institute for Nuclear Study, University of Tokyo

Tanashi, Tokyo 188, Japan

K. SAKAMOTO, Y. HAMAJIMA, M. SOTO, Y. KUBOTA, and M. YOSHIDA

Department of Chemistry, Faculty of Science, Kanazawa University

Kanazawa, Ishikawa 920, Japan

I. FUJIWARA*

Institute of Atomic Energy, Kyoto University

Uji, Kyoto 611, Japan

Abstract

Formation yields of 24 radioactive nuclides by the interaction of bremsstrahlung in the maximum end-point energies of 100 MeV - 1 GeV with Cu have been measured by direct γ-ray counting of irradiated targets. The yields in the mass range of 42 to 60 except for ^{60}Cu were analysed by non-linear least-squares fit to construct the mass yield and charge dispersion curves in spallation reactions. From the parameter values obtained, the energy dependence of the slope of the mass yield curve and the relationship between target N/Z and the most probable product N/Z were investigated in comparison with the results of proton, α and heavy ion-induced spallations of Cu. The characteristics of photon-induced spallations are discussed.

NUCLEAR REACTION: Cu(γ,spallation), E_{max} = 100 MeV - 1 GeV, measured formation yields 24 radioactive nuclides, deduced mass yield and charge dispersion curves, Ge(Li) and pure Ge detectors, natural target.

I. INTRODUCTION

For a number of years studies of high energy spallation reactions have yielded valuable information for not only the understanding of reaction mechanisms and nuclear properties but also the application to other fields such as cosmic rays.[1] However, studies of spallation of complex nuclei by high energy photons seem to be rather scanty in comparison with those by protons. In general, the mechanism of spallation reactions has been explained on the basis of the cascade-evaporation model suggested by Serber.[2] The incident projectile initiates a knockon cascade by the interaction with a nucleon inside the target nucleus, and a number of particles are ejected from the nucleus. The residual nucleus is deexcited by the evaporation of nucleons or clusters of the nucleus, and then the final product is formed.

In the case of photon incident, at higher energies than pion production threshold ($\sim$ 140 MeV), the Δ isobar is probably formed inside the target nucleus by the interaction of an incident photon with a nucleon in the nucleus. This isobar decays almost immediately into a nucleon and a pion. These two particles would usually develop a cascade process when they interact with other nucleons and clusters inside the nucleus. The final products are obtained after the deexcitation by the particle evaporation. The initial interaction in photospallation is quite different from that in proton spallation. Therefore, it is interesting whether or not the yield distribution of product nuclides is effected by this difference of the initial interaction between photon and proton incident on the same target nucleus.

In recent radiochemical studies of spallation reactions, it has been suggested that the logarithmic slope of the mass yield curve is an indirect measure of the average excitation energy transferred from the incident

particles, or the temperature of the cascade residues. A smaller slope corresponds to a higher average deposition energy. In proton and heavy ion (^{14}N, ^{12}C and ^{40}Ar) spallation reactions at E = 4 - 80 GeV of Cu by Cumming *et al.*,[3-5] it has been shown that the slope decreases with the increase of the kinetic energy of incident particles up to ~ 2 GeV and then approaches a constant value in the higher energy region than 2 GeV and that all of their slopes fall on the same curve. They have pointed out the problem why different projectiles give the same distribution of the excited system.

On the other hand, the results of photon-induced spallation reactions of V[6] and I[7] have shown that the slope of the mass yield curve decreases with the increase of the maximum end-point energy of bremsstrahlung up to 600 MeV and becomes constant in the higher energy region. This trend is appearently different from those observed in the hadron spallation reactions.

In this point of view, photon-induced spallations of Cu have been performed with bremsstrahlung in order to compare directly with the results of proton and heavy ion spallation reactions of Cu and also to confirm the trend obtained from photospallation reactions of V and I. In the present paper, we report the results by bremsstrahlung in maximum end-point energies of 100 MeV - 1 GeV. The results were analysed with the five-parameter formula given by Rudstam[8] according to Jonsson and Lindgren.[9,10] A special interest was paid for the energy dependence of the parameter P in the Rudstam's formula, to which the logarithmic slope of the mass yield curve is functionally equivalent.

II. EXPERIMENTAL PROCEDURES

The irradiations in the maximum bremsstrahlung energy region E_{max} = 300 MeV - 1 GeV in ~ 100 MeV step were performed at the 1.3 GeV electron synchrotron of Institute for Nuclear Study (INS), University of Tokyo, and those in the range E_{max} = 100 MeV - 250 MeV in ~ 30 MeV step and at E_{max} = 300 MeV were done at the 300 MeV and 500 MeV electron linear accelerators of Laboratory of Nuclear Science (LNS), Tohoku University and of Electrotechnical Laboratory (ETL), respectively.

At INS, an electron-free collimated bremsstrahlung beam from the internal target of Pt with 50 μm thickness of the synchrotron was used, and the beam spot was about 2 cm in diameter. The target Cu and monitor Al with size of 2.5 cm × 2.5 cm were prepared. Both purities are 99.99%, and their thicknesses were 450 mg/cm^2 and 270 mg/cm^2, respectively. The target stack consists of 4 - 8 Cu plates and an Al plate as an internal beam monitor. The target and monitor plates were guarded on both sides by Cu and Al foils, respectively, in order to compensate recoil losses and to prevent cross-contamination between target and monitor.

At LNS and ETL, an uncollimated beam was obtained from the Pt converter with 0.5 mm thickness of linear accelerators. The targets and monitors were cut into disks of 1 cm in diameter. Both purities are also 99.99% and their thicknesses were 18 mg/cm^2 and 7 mg/cm^2, respectively. Those disks including guard foils wrapped with Al foil of 2 mg/cm^2 were stacked in a quartz tube and irradiated in a water cooled target holder at LNS.[11,12] Irradiations at ETL were the same as those at LNS except for irradiating in air.

The absolute yields (mb per equivalent quantum) for the monitor reaction ^{27}Al(γ,2pn)^{24}Na have already been reported by various authors.[13-18] However, the scattering of the data are appreciable. The difference between the highest yield and the lowest at the same maximum end-point energy seems to attain about 40%.

Therefore, the beam intensity was also measured by means of a calibrated quantameter placed several meters behind the target stack in the irradiation of E_{max} = 850 MeV at INS. Consequently, we adopted the data for the monitor reaction given by Johnsson *et al.*[13] as the intensity monitor, because of the agreement with the intensity measured by the quantameter within an experimental uncertainty. In other irradiations at INS, the beam intensity was monitored only by the $^{27}Al(\gamma,2pn)^{24}Na$ reaction since another target stack was always placed behind the Cu stack. At LNS, C foils were also used as a monitor by the reaction of $^{12}C(\gamma,n)^{11}C$.[19] The photon intensities were 10^{8} - 10^{9} eq.q./sec at INS and 10^{12} - 10^{13} eq.q./sec at LNS and ETL, and typical irradiation times were 4 hr at INS and 5 min at LNS and ETL, respectively.

After irradiation, γ rays from Cu target plates or foils and monitors were measured directly with pure Ge and Ge(Li) detectors with the energy resolution of 1.8 keV FWHM at 1332 keV connected to multichannel pulse height analysers. The detection efficiencies of detectors were measured by γ-ray reference sources with a point spot and corrected for the target or monitor thickness and the size of the beam spot by the computer program.[20] The radioactive nuclides produced in irradiations were identified by their half-lives and energies of emitted γ rays. Their relevant properties[21] are tabulated in Table I. The measurements were continued for more than one month. The γ-ray spectra were analysed with the peak search program[22] using FACOM M380 at INS.

The contribution from secondary particles in irradiations should always be considered. At E_{max} = 850 MeV, the depth profiles of radioactivities induced in Cu stack were investigated. The results are shown in Fig.1. In this irradiation, no serious effects were observed in the spallation yields of product nuclides. However, the yields of the spallation products such as ^{54}Mn and ^{48}Sc slightly decreased with the increase of the target thickness. It may be due to the

decrease of the average energy of the incident bremsstrahlung with the increase of the target thickness. Furthermore, another sample was always placed off the beam line in irradiations, and it was found that the yield was negligibly small compared with that in the target placed on the beam line. Therefore, two or three Cu target plates or foils placed on the upstream side for the incident photons were used in the measurements.

III. RESULTS

The measured production yields are listed in Table II. Each yield is identified as being independent(I) or cumulative(C) in the table, and is the average of separate measurements by pure Ge and Ge(Li) detectors. These yields were calculated for the natural isotopic abundance of copper.

The errors associated with the yields refer to counting statistics, detector efficiencies of γ rays and decay curve analyses. Systematic uncertainties due to the beam intensity calibration which were estimated to be approximately 15% are not included in the quoted errors. Duplicate runs were also performed at E_{max} = 400, 500, 600, 700, 900 and 1000 MeV, and their results agreed well with those listed in Table II.

The yields of ^{61,64}Cu, the (γ,xn) reaction products were almost constant in the energy region of E_{max} = 100 MeV - 1 GeV within an experimental error. These nuclides were predominantly produced by giant resonance and quasi-deuteron process induced by lower energy photons than $\sim$ 100 MeV. Also, the yields for spallation products at $E_{max} \leq$ 250 MeV measured at LNS are smoothly connected with those at $E_{max} \geq$ 310 MeV measured at INS. The yields at E_{max} = 305 MeV at

ETL seem to be consistent with those at E_{max} = 310 MeV at INS. Therefore, it indicates the consistency between the yields from the linear accelerators and those from the synchrotron. The present yields are also compatible with the data by bremsstrahlung at E_{max} = 2 GeV.[23]

IV. ANALYSIS AND DISCUSSION

Least-squares fit

The obtained spallation yields were analysed in order to systematize by the five-parameter formula (CDMD) given by Rudstam,[8]

$$\sigma(Z,A) = \frac{\hat{\sigma}\ P\ R^{2/3}}{1.79(e^{P A_t} - 1)} \exp\{P A - R\,|\,Z - S A + T A^2|^{3/2}\} \qquad (1)$$

where $\sigma(Z,A)$ is the yield for a nuclide(Z,A) produced from the target (Z_t, A_t). P, R, S, T and $\hat{\sigma}$ are free parameters. P defines the slope of the mass yield curve, R the width of the charge dispersion curve, S and T are related to the most probable charge Z_p of the charge dispersion by $Z_p = SA - TA^2$ and $\hat{\sigma}$ the total inelastic yield, respectively. The product mass range used in the analysis was limited to $42 \leq A \leq 60$ except for ^{60}Cu in order to prevent the contribution from other reaction processes such as fragmentation and simple reaction. The yields of ^{57}Co were corrected for the decay of ^{57}Ni. Recently, some modified forms[3-5,24,25] of the Rudstam's formula have been used for the analysis. Ku and Karol[26] have analysed the results of α-induced spallation reactions by applying

the skewed Gaussian function to the fitting of the isobaric yield distribution by considering the yields of neutron rich product nuclides. However, we selected the original form of the formula with the symmetric charge distribution in order to compare with the results calculated by Jonsson and Lindgren,[9,10] who have compiled the parameters for some photospallation yields analysed by the CDMD formula and proposed the relations to calculate the parameters of the Rudstam's formula. Among the relations, the expressions for the parameter P,

$$P = 1460\ E_{max}^{-0.81}\ A_f^{-0.69} \text{ for } E_{max} \leq 600\text{MeV} \quad (2)$$

$$P = 7.66\ A_f^{-0.69} \text{ for } E_{max} > 600\ \text{MeV} \quad (3)$$

are different from that for proton spallations.

The parameters were calculated by a non-linear least-squares fit to the experimentally obtained spallation yields. The fitting method has been described in detail in ref.27, which is basically the same as that suggested by Rudstam.[8] The parameters obtained by this method are given in Table III with other results of photospallations of Cu.[23,28] The results of the fit at E_{max} = 850 MeV are shown as an example in Fig.2. The solid curves were calculated by the formula using the obtained parameter values. It was certified that the slope of the mass yield curve and the peak position of the charge dispersion curve are almost independent of fitting methods, although the width of the charge dispersion curve could be somewhat effected by methods.

Slope of mass yield curve

In Fig.3, the parameter P's obtained by the fit are plotted and slightly lower than values estimated from the relations (2) and (3), which is shown by the dashed line. However, this result shows the same trend as those by V and I photospallations; the P decreases with the increase of the maximum bremsstrahlung energy up to 600 MeV and then approaches a constant value in the higher energy region. In this figure, the slopes of the mass yield curve in proton and heavy ion spallations of Cu obtained by Cumming *et al.*[3-5] are shown in the solid line, in which the result of α-induced spallation reactions of Cu^{29} is also included. The parameter P's estimated by Rudstam[6] for a number of proton (and some neutron, deuteron and α) spallations of medium weight target nuclei are also indicated by the dash-dotted line. The results by Cumming *et al.*[3-5] and Rudstam[6] are almost consistent with each other. The slopes or P's obtained in hadron spallations of the same target nucleus fall on the same single curve and their energy dependence is lost in the energy region more than about 2 GeV. Therefore, two different points between photon and hadron- induced spallations are deduced as follows.

(1) The slope of the mass yield curve (P) approaches constant at energies of more than 600 MeV in the photospallation while more than 2 GeV in the hadron spallation.

(2) The slope values of photospallation are larger than those of hadron spallation.

Since the work of photospallation has to depend on bremsstrahlung with a continuous energy spectrum as a photon source, the present results should be converted to those by monochromatic photons. The mean cross sections (mb) in the energy region of 300 - 1000 MeV were estimated from the yields (mb/eq.q.) in the assumption of 1/E dependence of the bremsstrahlung spectrum according to Jonsson and Persson.[7] The parameters obtained for these cross sections were almost

identical with those at E_{max} = 600 and 700 MeV. It does not seem that the P decreases to the same value as that of the hadron spallation by the conversion of yield to cross section. However, it could be described qualitatively that afetr the conversion the slope (P) would approach constant around 600 MeV or less because the mean energy of the interacting photons is less than the maximum end-point energy.

The slope of the mass yield curve is an indirect measure of the energy deposition by the incident particles or photons. From the slope data, the excitation energy seems to be saturated in higher kinetic energy than 2 GeV in hadron reactions, while less than 600 MeV in the photon reactions. Furthermore, it shows that the saturated excitation energy is higher in hadron spallation than in photon in this incident energy region. It would seem plausible that the different points (1) and (2) would partly be induced by the difference of the initial interaction between photon and proton spallations because the threshold energy of pion production in photon-nucleon interaction is lower than that in nucleon-nucleon interaction. Further experimental and theoretical investigations are required.

In pion-induced spallation reactions,[30,31] the slope values plotted as a function of the energy corresponding to the sum of their kinetic energy and the rest mass energy show a similar trend as the Cumming's solid curve in Fig.3. The average excitation energy of cascade residues estimated from the slope of the mass yield curve is in the relation of $\gamma < p = \alpha =$ heavy ion $= \pi^-$ in several hundreds MeV to several GeV energy region. Therefore, photospallations appearently show different characteristics from hadron spallations.

The target mass dependence of the slope (P) shown by relations (2) and (3) was also confirmed by our results of photospallations of Y, I, Cs and Au. These results will be published soon elsewhere.[32]

Charge dispersion curve

The charge dispersion curve obtained at E_{max} = 850 MeV is shown in Fig.4 as an example. The unmeasured yields of stable and long-lived products were estimated from the CDMD formula by the parameters obtained and all of the yields were converted to the relative yields in the product mass chain. In the figure, the curve for 3.9 GeV proton spallation of Cu by Cumming *et al.*[3] is shown by the dashed curve, which is vertically shifted to superpose at the peak position of photospallation. The absolute yields of hadron spallations are larger than those of the photospallations, and the width of the charge dispersion curve of photospallation is slightly narrower than that of the proton spallation. The width of the charge dispersion curve can also be effected by the value of the power of $(Z - SA + TA^2)$. We also performed the analysis using 2 instead of 3/2 for the value of the power, which corresponds to the CDMD-G formula, since Cumming *et al.* have used 2 for it. As the value for R, we obtained 1.78 at E_{max} = 850 MeV ,and other parameter values were identical for those by the CDMD formula. The result by the CDMD-G is shown by the thin solid curve in the figure, which seems to be still narrower than that of proton spallation. If it is true, this supports the investigation for the difference of the average excitation energy of cascade residues between photospallations and hadron ones described in the previous section. Unfortunately, these curves overlap with one another in $|Z_p - Z| > 1.3$. Therefore, it is required for the discussion to measure yields of neutron rich and deficient products accurately.

Most probable charge Z_p

From the parameters S and T, the most probable product N/Z was estimated by the following relations,

$$Z_p = S A_a - T A_a^2 \tag{4}$$

$$A_a = A_t - 1/P \tag{5}$$

and was constant within an experimental error in the maximum energy region of 100 MeV - 1 GeV. The average value of 1.148 ± 0.003 was obtained. The result is shown in Fig.5 as a function of target N/Z together with those of 1.8,[33] 2.9[34] and 12 GeV[25] proton and 720 MeV α spallations[28] of targets with various values of N/Z. In this figure, the results obtained by the photospallations of V[9,10] and I[7] are also plotted, which are average values in E_{max} = 100 - 800 MeV and 250 - 1000 MeV, respectively. Furthermore, our data of photospallations of Y, I, Cs and Au are also shown in the figure. It is found that there exists a nearly linear relationship between target N/Z and the most probable product N/Z in each spallation by photon and proton (and α) and that the slope for photospallations is steeper than that for proton and α spallations. In larger values of target N/Z, the most probable product N/Z is shifted to more neutron rich side in photospallations than in proton and α spallations. Solid and dashed lines in the figure, which are for eye guide, cross around target N/Z of about 1.2. Our result for the most probable product N/Z of the photospallation of Cu agreed well with those of hadron spallations of Cu.[3-5,25,29]

It seems to be related this phenomenon with the average excitation energy of cascade residues produced by spallations. At the end of the cascade process,

the ratio N/Z of the cascade residues is approximately equal to the target N/Z. As the cascade residues are deexcited by the evaporation, the Coulomb barrier becomes to suppress the emission of protons and charged particles. Since the average excitation energy of cascade residues in photospallations is lower than that in hadron spallations, which is also evidenced by the difference of the parameter P between photon and hadron spallations, the emission of nucleons is relatively limited in photospallations. Therefore, the most probable N/Z is higher in photospallations than in proton and α spallations. Although it is easy to find this phenomenon in neutron rich nucleus as a target, it seems to be difficult in the medium-wight nucleus such as Cu of which N/Z is near unity.

ACKNOWLEDGEMENTS

The authors are indebted to Drs. M. Yagi, K. Masumoto and T. Mitsugashira of Tohoku University, to Drs. T. Tomimasu, Y. Kawada and Y. Hino of ETL, to the operation crew of the synchrotron at INS and to Dr. K. Yamakoshi of University of Tokyo for their invaluable cooperations in the accelerator operations and/or the radioactivity measurements.

*Present address: School of economics, Ottemon-gakuin University, Ibaragi, Osaka 567, Japan.

References

1. For example, see *High-Energy Nuclear Reactions in Astrophysics*, edited by B.S.P. Shen (Benjamin, New York 1967) and *Spallation Nuclear Reactions and Their Applications*, edited by B.S.P. Shen (Reidel, Boston, 1976).
2. R. Serber, Phys. Rev. 72, 1114 (1947).
3. J.B. Cumming, P.E. Haustein and R.W. Stoenner, Phys. Rev. C10, 739 (1974).
4. J.B. Cumming, R.W. Stoenner and P.E. Haustein, Phys. Rev. C14, 1554 (1976).
5. J.B. Cumming, P.E. Haustein, T.J. Ruth and G.J. Virts, Phys. Rev. C17, 1632 (1978).
6. B. Bülow, B. Johnsson, M. Nilsson and B. Forkman, Z. Phys. A278, 89 (1976).
7. G.G. Jonsson and B. Persson, Nucl. Phys. A153, 32 (1970).
8. G. Rudstam, Z. Naturforsch. 21a, 1027 (1966).
9. G.G. Jonsson and K. Lindgren, Physica Scripta 7, 49 (1973).
10. G.G. Jonsson and K. Lindgren, Physica Scripta 15, 308 (1977).
11. K. Sakamoto, H. Toramoto, Y. Hamajima, K. Okada and M. Dohniva, Radiochim. Acta 37, 89 (1984).
12. K. Sakamoto, M. Nishio, M. Dohniva, K. Okada and Y. Hamajima, Radiochim. Acta 37, 83 (1984).
13. B. Johnsson, A. Järund and B. Forkman, Z. Phys. A273, 97 (1975).
14. G. Andersson, I. Blomqvist, B. Forkman, G.G. Jonsson, A. Järund, I. Kroon, K. Lindgren, B. Schrøder and K. Tesch, Nucl. Phys. A197, 44 (1972).
15. G. Kumbartzki, U. Kim and Ch.K. Kwan, Nucl. Phys. A160, 237 (1971).
16. A. Järund, B. Friberg and B. Forkman, Z. Phys. 262, 15 (1973).
17. A. Masaike, J. Phys. Soc. Jpn., 19, 427 (1964).
18. N.di Napoli, A.M. Lacerenza, F. Salvetti, H.G.de Carvalho and J. Benuzzi-Martins, Lett. Nuovo Cimento 1, 835 (1971).

19. G. Hyltén, Nucl. Phys. A158, 225 (1970).

20. T. Nakamura, Nucl. Instr. and Meth. 131, 521 (1975).

21. C.M. Lederer and V.S. Shirley, *Table of Isotopes* (Wiley, New York, 1978), 7th ed.

22. K. Komura, Technical Report of Institute for Nuclear Study, University of Tokyo, INS-TCH 9 (1974) (unpublished).

23. N.M. Bachschi, P. David, J. Debrus, F. Lübke, H. Mommsen, R. Schoenmackers, G.G. Jonsson and K. Lindgren, Nucl. Phys. A264, 493 (1976).

24. N.T. Porile, G.D. Cole and C.R. Rudy, Phys. Rev. C19, 2288 (1979).

25. T. Asano, Y. Asano, Y. Iguchi, H. Kudo, S. Mori, M. Noguchi, Y. Takada, H. Hirabayashi, H. Ikeda, K. Katoh, K. Kondo, M. Takasaki, T. Tominaka and A. Yamamoto, Phys. Rev. C28, 1718 (1983).

26. T.H. Ku and P.J. Karol, Phys. Rev. C16, 1984 (1977).

27. Y. Kubota, Master Thesis, Kanazawa University, 1986 (unpublished).

28. The data were cited in ref. 7 as G.G. Jonsson preliminary results.

29. P.J. Karol, Phys. Rev. C10, 150 (1974).

30. P.E. Haustein and T.J. Ruth, Phys. Rev. C18, 2241 (1978).

31. T. Nishi, I. Fujiwara, N. Imanishi, H. Moriyama, K. Otozai, R. Arakawa, T. Saito, T. Tsuneyoshi, N. Takahashi, S. Iwata, S. Hayashi, S. Shibata, H. Kudo and K. Yoshida, Bull. Inst. Chem. Res., Kyoto University, 60, 132 (1982).

32. K. Sakamoto, Y. Hamajima, M. Soto, Y. Kubota, M. Yoshida, T. Hashimoto, T. Fukasawa, I. Fujiwara and S. Shibata, Research Report of Laboratory of Nuclear Science, Tohoku University, 18, 290 (1985) (to be published).

33. S. Kaufman, Phys. Rev. 129, 1866 (1963)

34. N.T. Porile and L.B. Church, Phys. Rev. 133, B310 (1964).

Figure Captions

Fig.1. Variations of some radioactivities produced in a thick Cu target stack irradiated at E_{max} = 850 MeV.

Fig.2. Yield distributions for products in the mass range $42 \leq A \leq 60$ except for ^{60}Cu from Cu(γ,spallation) reactions at E_{max} = 850 MeV. Solid curves are obtained by the parameters estimated by non-linear least-squares fit to the yield data.

Fig.3. Logarithmic slope of the mass yield curve (P) as a function of maximum bremsstrahlung energy or kinetic energy of nuclear projectiles. (●)-this work, (△)-ref.28, (▽)-ref.23. The thin solid curve is for eye guide for the results of this work. The dashed line was estimated for Cu target from the relations (2) and (3) in the text. The thick solid curve is for the slopes obtained by Cumming *et al.*[3-5] for Cu target. Results for α-induced spallations of Cu[29] are also included in this curve. The dash-dotted line is for P values obtained by Rudstam[8].

Fig.4. Charge dispersion curve at E_{max} = 850 MeV. The symbols are the same as those in Fig.2. The dashed curve is for 3.9 GeV proton spallations of Cu,[3] and the thin solid curve is obtained by the analysis of the CDMD-G formula. They are vertically shifted to superpose at the peak position of the thick solid curve obtained by the CDMD formula.

Fig.5. Most probable product N/Z as a function of target N/Z. Open symbols represent photon results and filled proton and α results. (○)-this work, (△)-ref.10 (V target), (▽)-ref.7 (I), (□)-ref.32 (Y, I, Cs and Au), (●)-ref.34 (^{96}Zr, ^{98}Mo and ^{96}Ru). (▲)-ref.25 (Ti, Fe, Co, Ni, Cu and Zn), (▼)-ref.33 (In and Au), (■)-ref.28 (^{92}Mo, ^{98}Mo and ^{100}Mo). The solid and dashed lines are for eye guide. A part of the results for proton and α spallations was reproduced from ref. 28.

TABLE I. Relevant properties of nuclides measured.

Nuclide	Half-life	Radiation measured	Fractional abundance
Cu-64	12.71 h	1346 keV	0.62 %
Cu-61	3.37 h	283	13.3
		656	11.8
Cu-60	23.0 m	1333	87.9
		1792	45.4
Ni-57	36.1 h	1378	77.7
Co-60	5.27 y	1173	100
		1333	100
Co-58	70.8 d	811	99.4
Co-57	271 d	122	85.6
Co-56	78.5 d	847	99.95
Co-55	17.5 h	1408	16.5
Fe-59	44.6 d	1099	56.5
Mn-56	2.58 h	1811	27.3
Mn-54	312.5 d	835	100
Mn-52	5.63 d	744	90
		1434	100
Cr-51	27.7 d	320	10.2
Cr-49	42 m	91	51.3
		153	29.2
V -48	15.98 d	984	100
Sc-48	43.7 h	1038	97.5
Sc-47	3.41 d	159	68.5
Sc-46	83.8 d	889	100
Sc-44m	58.6 h	272	86.6
Sc-44	3.93 h	1157	99.89
K -43	22.3 h	373	87.8
K -42	12.36 h	1525	18.8
Na-24	15.02 h	1369	100

TABLE II. Formation yield (mb/eq. q.) for photon-induced spallation reaction of Cu.

Product	100 MeV	130 MeV	160 MeV	220 MeV
Cu-64 (I)	15.9 ± 1.1	15.9 ± 0.9	16.0 ± 1.0	14.8 ± 1.1
Cu-61 (I)	3.31 ± 0.17	3.39 ± 0.18	3.39 ± 0.18	3.10 ± 0.16
Cu-60 (I)	0.199 ± 0.018	0.217 ± 0.019	0.217 ± 0.018	0.256 ± 0.030
Ni-57 (C)	0.005 ± 0.001	0.007 ± 0.001	0.012 ± 0.001	0.014 ± 0.002
Co-60 (I)	0.418 ± 0.034	0.470 ± 0.044	0.484 ± 0.040	0.602 ± 0.043
Co-58 (I)	0.750 ± 0.038	0.882 ± 0.043	0.816 ± 0.039	1.18 ± 0.06
Co-57 (C)	0.256 ± 0.013	0.341 ± 0.017	0.352 ± 0.018	0.570 ± 0.029
Co-56 (C)	0.035 ± 0.002	0.053 ± 0.003	0.068 ± 0.004	0.133 ± 0.007
Co-55 (C)	—	—	—	0.023 ± 0.005
Fe-59 (C)	0.018 ± 0.001	0.021 ± 0.002	0.023 ± 0.002	0.040 ± 0.003
Mn-56 (C)	0.011 ± 0.001	0.020 ± 0.002	0.028 ± 0.003	0.047 ± 0.004
Mn-54 (I)	0.040 ± 0.003	0.068 ± 0.006	0.093 ± 0.006	0.219 ± 0.012
Mn-52 (C)	0.002 ± 0.001	0.004 ± 0.001	0.009 ± 0.001	0.034 ± 0.002
Cr-51 (C)	0.006 ± 0.001	0.013 ± 0.002	0.022 ± 0.002	0.098 ± 0.008
Cr-49 (C)	—	—	—	—
V -48 (C)	—	—	—	0.013 ± 0.002
Sc-48 (I)	—	—	—	—
Sc-47 (C)	—	—	—	—
Sc-46 (I)	—	—	—	—
Sc-44m(I)	—	—	—	—
Sc-44 (I)	—	—	—	—
K -43 (C)	—	—	—	—
K -42 (I)	—	—	—	—
Na-24 (C)	—	—	—	—

TABLE II. (continued)

Product	250 MeV	305 MeV	310 MeV
Cu-64 (I)	15.6 ± 0.9	17.0 ± 0.9	17.2 ± 1.3
Cu-61 (I)	3.74 ± 0.21	3.54 ± 0.18	3.46 ± 0.18
Cu-60 (I)	0.266 ± 0.021	—	0.196 ± 0.015
Ni-57 (C)	0.021 ± 0.002	0.024 ± 0.002	0.034 ± 0.005
Co-60 (I)	0.852 ± 0.062	0.607 ± 0.057	0.627 ± 0.188
Co-58 (I)	1.39 ± 0.07	1.28 ± 0.03	1.31 ± 0.07
Co-57 (C)	0.726 ± 0.037	0.766 ± 0.016	0.826 ± 0.062
Co-56 (C)	0.169 ± 0.009	0.185 ± 0.006	0.230 ± 0.027
Co-55 (C)	0.023 ± 0.004	0.031 ± 0.006	—
Fe-59 (C)	0.050 ± 0.004	0.052 ± 0.002	0.042 ± 0.010
Mn-56 (C)	0.056 ± 0.005	0.080 ± 0.005	0.077 ± 0.009
Mn-54 (I)	0.308 ± 0.017	0.388 ± 0.005	0.480 ± 0.069
Mn-52 (C)	0.050 ± 0.003	0.085 ± 0.006	0.083 ± 0.006
Cr-51 (C)	0.145 ± 0.011	0.255 ± 0.009	0.247 ± 0.043
Cr-49 (C)	—	—	—
V -48 (C)	0.023 ± 0.002	0.057 ± 0.004	0.072 ± 0.008
Sc-48 (I)	—	—	—
Sc-47 (C)	—	0.014 ± 0.003	0.014 ± 0.003
Sc-46 (I)	—	0.024 ± 0.004	0.022 ± 0.010
Sc-44m(I)	—	—	0.012 ± 0.002
Sc-44 (I)	—	—	0.011 ± 0.003
K -43 (C)	—	—	—
K -42 (I)	—	—	—
Na-24 (C)	—	—	—

TABLE II. (continued)

Product	400 MeV	500 MeV	600 MeV	700 MeV
Cu-64 (I)	16.9 ± 1.2	17.4 ± 1.2	16.6 ± 1.0	16.5 ± 1.0
Cu-61 (I)	3.48 ± 0.18	3.61 ± 0.18	3.48 ± 0.18	3.39 ± 0.17
Cu-60 (I)	0.220 ± 0.015	0.209 ± 0.013	0.228 ± 0.013	0.218 ± 0.012
Ni-57 (C)	0.039 ± 0.004	0.042 ± 0.005	0.040 ± 0.003	0.040 ± 0.004
Co-60 (I)	0.966 ± 0.372	1.06 ± 0.30	1.24 ± 0.28	1.06 ± 0.09
Co-58 (I)	1.75 ± 0.05	1.96 ± 0.06	2.04 ± 0.10	2.03 ± 0.09
Co-57 (C)	0.986 ± 0.013	1.25 ± 0.05	1.27 ± 0.04	1.32 ± 0.04
Co-56 (C)	0.310 ± 0.021	0.366 ± 0.016	0.406 ± 0.025	0.397 ± 0.022
Co-55 (C)	0.045 ± 0.004	0.039 ± 0.009	0.065 ± 0.009	0.046 ± 0.007
Fe-59 (C)	0.072 ± 0.012	0.106 ± 0.008	0.114 ± 0.019	0.117 ± 0.011
Mn-56 (C)	0.103 ± 0.009	0.145 ± 0.010	0.151 ± 0.010	0.154 ± 0.009
Mn-54 (I)	0.599 ± 0.042	0.828 ± 0.034	0.869 ± 0.038	0.900 ± 0.039
Mn-52 (C)	0.147 ± 0.008	0.199 ± 0.011	0.227 ± 0.008	0.228 ± 0.013
Cr-51 (C)	0.490 ± 0.034	0.596 ± 0.038	0.737 ± 0.043	0.774 ± 0.060
Cr-49 (C)	0.031 ± 0.005	0.043 ± 0.004	0.051 ± 0.005	0.052 ± 0.004
V -48 (C)	0.123 ± 0.008	0.179 ± 0.007	0.225 ± 0.009	0.266 ± 0.023
Sc-48 (I)	0.009 ± 0.002	0.017 ± 0.003	0.018 ± 0.002	0.015 ± 0.003
Sc-47 (C)	0.029 ± 0.012	0.044 ± 0.002	0.053 ± 0.003	0.054 ± 0.004
Sc-46 (I)	0.069 ± 0.020	0.095 ± 0.008	0.131 ± 0.012	0.121 ± 0.010
Sc-44m(I)	0.026 ± 0.002	0.044 ± 0.003	0.057 ± 0.003	0.064 ± 0.005
Sc-44 (I)	0.024 ± 0.003	0.043 ± 0.005	0.051 ± 0.005	0.058 ± 0.007
K -43 (C)	—	—	0.017 ± 0.003	0.012 ± 0.002
K -42 (I)	—	—	0.037 ± 0.006	0.038 ± 0.007
Na-24 (C)	—	0.003 ± 0.001	0.005 ± 0.001	0.006 ± 0.001

TABLE II. (continued)

Product	800 MeV	850 MeV	900 MeV	1000 MeV
Cu-64 (I)	16.6 ± 1.0	17.7 ± 0.5	15.7 ± 1.0	16.8 ± 1.0
Cu-61 (I)	3.60 ± 0.18	3.55 ± 0.09	3.38 ± 0.17	3.51 ± 0.18
Cu-60 (I)	0.240 ± 0.013	0.213 ± 0.009	0.211 ± 0.011	0.252 ± 0.013
Ni-57 (C)	0.046 ± 0.003	0.044 ± 0.002	0.046 ± 0.003	0.052 ± 0.003
Co-60 (I)	1.11 ± 0.13	—	1.14 ± 0.14	1.08 ± 0.16
Co-58 (I)	2.04 ± 0.05	2.26 ± 0.06	2.26 ± 0.07	2.44 ± 0.08
Co-57 (C)	1.34 ± 0.04	1.46 ± 0.04	1.40 ± 0.05	1.48 ± 0.05
Co-56 (C)	0.403 ± 0.018	0.367 ± 0.010	0.448 ± 0.017	0.495 ± 0.022
Co-55 (C)	0.070 ± 0.008	0.057 ± 0.003	0.061 ± 0.010	0.070 ± 0.009
Fe-59 (C)	0.108 ± 0.008	0.115 ± 0.005	0.162 ± 0.009	0.147 ± 0.031
Mn-56 (C)	0.167 ± 0.010	0.156 ± 0.004	0.161 ± 0.010	0.172 ± 0.009
Mn-54 (I)	0.996 ± 0.037	1.02 ± 0.03	1.04 ± 0.04	1.10 ± 0.04
Mn-52 (C)	0.252 ± 0.010	0.237 ± 0.006	0.261 ± 0.011	0.282 ± 0.014
Cr-51 (C)	0.841 ± 0.055	0.874 ± 0.026	0.852 ± 0.037	0.998 ± 0.039
Cr-49 (C)	0.057 ± 0.004	0.057 ± 0.003	0.054 ± 0.003	0.061 ± 0.004
V -48 (C)	0.259 ± 0.011	0.272 ± 0.007	0.309 ± 0.026	0.311 ± 0.022
Sc-48 (I)	0.016 ± 0.001	0.015 ± 0.001	0.023 ± 0.002	0.029 ± 0.002
Sc-47 (C)	0.061 ± 0.003	0.064 ± 0.002	0.071 ± 0.004	0.072 ± 0.003
Sc-46 (I)	0.155 ± 0.008	0.147 ± 0.005	0.165 ± 0.009	0.186 ± 0.008
Sc-44m(I)	0.079 ± 0.005	0.080 ± 0.003	0.085 ± 0.004	0.090 ± 0.005
Sc-44 (I)	0.069 ± 0.007	0.067 ± 0.005	0.070 ± 0.006	0.073 ± 0.007
K -43 (C)	0.013 ± 0.002	0.016 ± 0.001	—	0.022 ± 0.003
K -42 (I)	0.047 ± 0.006	0.047 ± 0.003	0.037 ± 0.008	0.056 ± 0.009
Na-24 (C)	0.006 ± 0.001	0.007 ± 0.001	0.007 ± 0.001	0.008 ± 0.002

TABLE III. Parameter values for formula (1) obtained from yield data.

E_{max} (MeV)	$\hat{\sigma}$	P	R	S	T
100	58 ± 11	0.69 ± 0.05	2.46 ± 0.10	0.486 ± 0.014	0.00033 ± 0.00025
130	51 ± 13	0.58 ± 0.05	2.39 ± 0.14	0.476 ± 0.020	0.00017 ± 0.00034
160	36 ± 7	0.50 ± 0.04	2.22 ± 0.12	0.474 ± 0.016	0.00013 ± 0.00029
220	34 ± 6	0.39 ± 0.04	2.21 ± 0.13	0.489 ± 0.013	0.00039 ± 0.00023
250	37 ± 6	0.35 ± 0.04	2.20 ± 0.13	0.493 ± 0.014	0.00048 ± 0.00024
305	26 ± 2	0.26 ± 0.02	2.03 ± 0.09	0.490 ± 0.009	0.00041 ± 0.00016
310	26 ± 2	0.25 ± 0.01	2.03 ± 0.11	0.470 ± 0.008	0.00006 ± 0.00015
400	32 ± 2	0.21 ± 0.01	2.08 ± 0.08	0.470 ± 0.008	0.00006 ± 0.00014
500	38 ± 2	0.19 ± 0.01	1.91 ± 0.09	0.476 ± 0.005	0.00017 ± 0.00009
600	39 ± 3	0.17 ± 0.01	2.08 ± 0.11	0.474 ± 0.005	0.00013 ± 0.00010
700	41 ± 3	0.18 ± 0.01	2.01 ± 0.10	0.481 ± 0.005	0.00027 ± 0.00010
800	40 ± 2	0.16 ± 0.01	1.95 ± 0.08	0.481 ± 0.004	0.00026 ± 0.00008
850	42 ± 3	0.16 ± 0.01	2.07 ± 0.09	0.479 ± 0.004	0.00024 ± 0.00008
900	44 ± 4	0.16 ± 0.01	1.96 ± 0.10	0.480 ± 0.006	0.00025 ± 0.00011
1000	45 ± 3	0.15 ± 0.01	2.07 ± 0.10	0.473 ± 0.005	0.00011 ± 0.00009
750[28]	—	0.21 ± 0.03	1.3 ± 0.5	0.48 ± 0.02	0.0002 ± 0.0001
2000[23]	72 ± 12	0.16 ± 0.02	2.4 ± 0.2	0.478 ± 0.006	0.0002 ± 0.0001

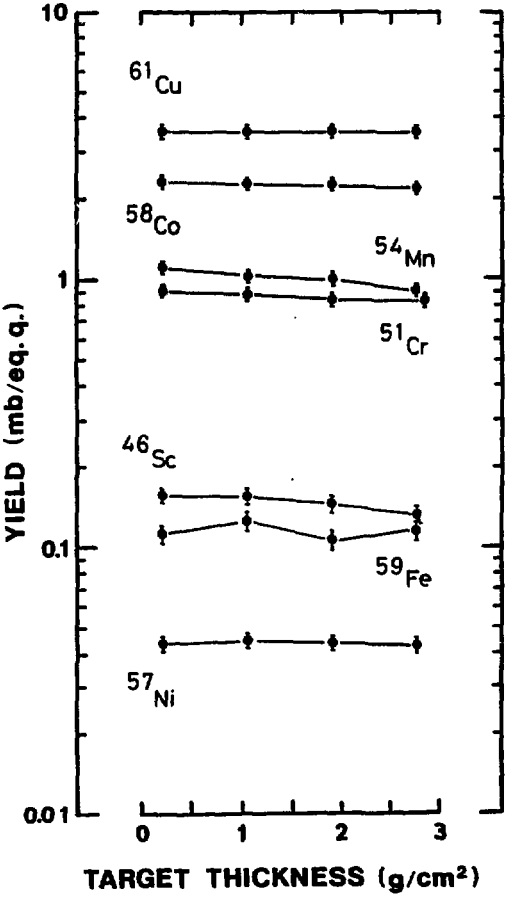
10
1
0.1
0.01
YIELD (mb/eq.q.)
61Cu
58Co
54Mn
51Cr
46Sc
59Fe
57Ni
0
1
2
3
TARGET THICKNESS (g/cm²)

Fig. 1

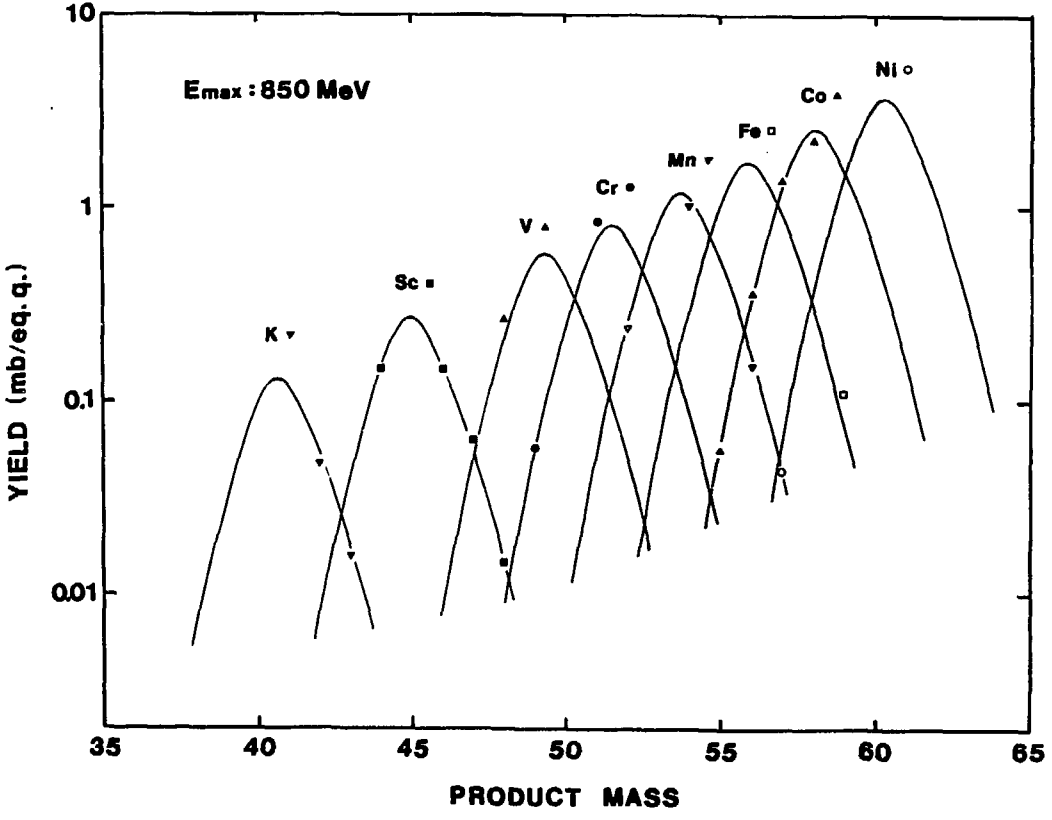
Emax : 850 MeV
K
Sc
V
Cr
Mn
Fe
Co
Ni
YIELD (mb/eq. q.)
PRODUCT MASS
10
1
0.1
0.01
35
40
45
50
55
60
65

Fig. 2

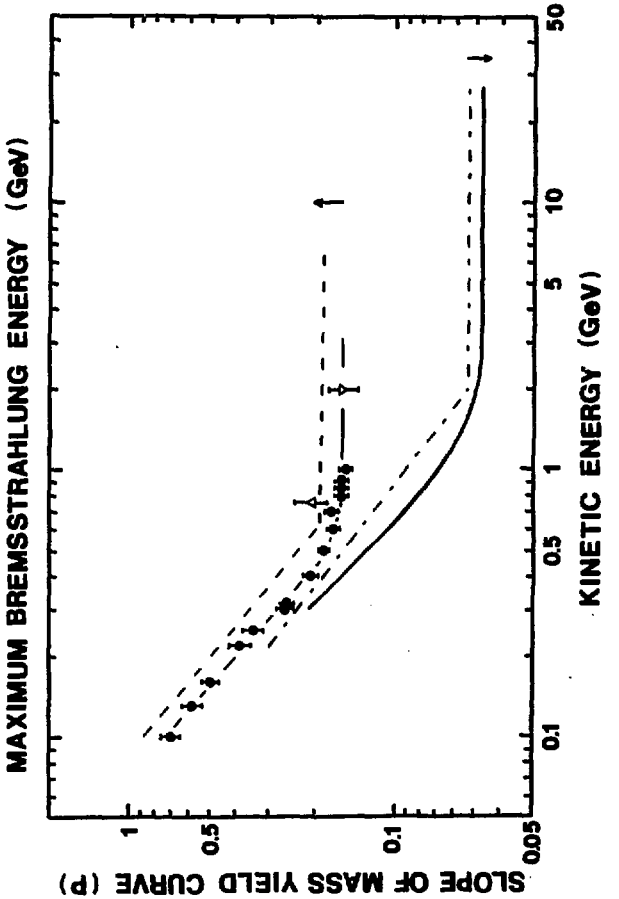
MAXIMUM BREMSSTRAHLUNG ENERGY (GeV)
SLOPE OF MASS YIELD CURVE (p)
KINETIC ENERGY (GeV)
1
0.5
0.1
0.05
0.1
0.5
1
5
10
50

Fig. 3

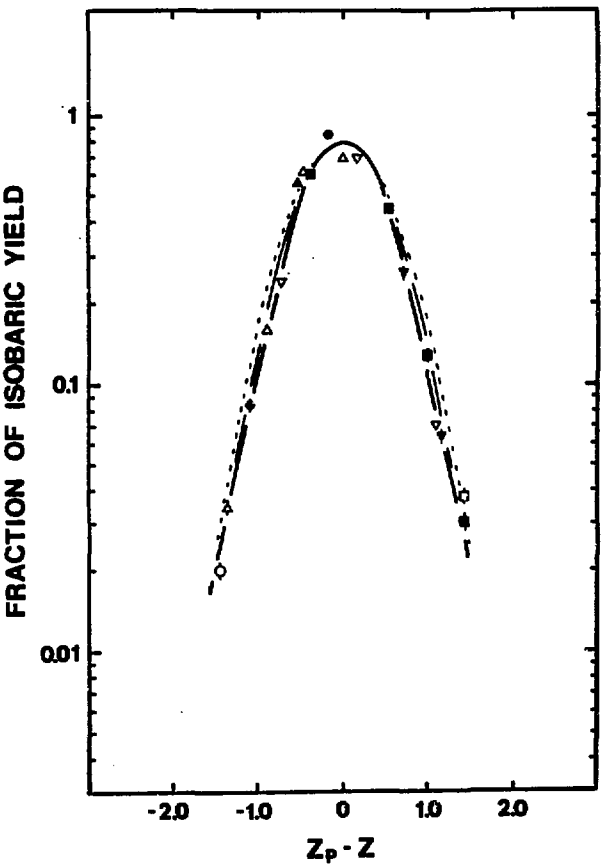

Fig. 4

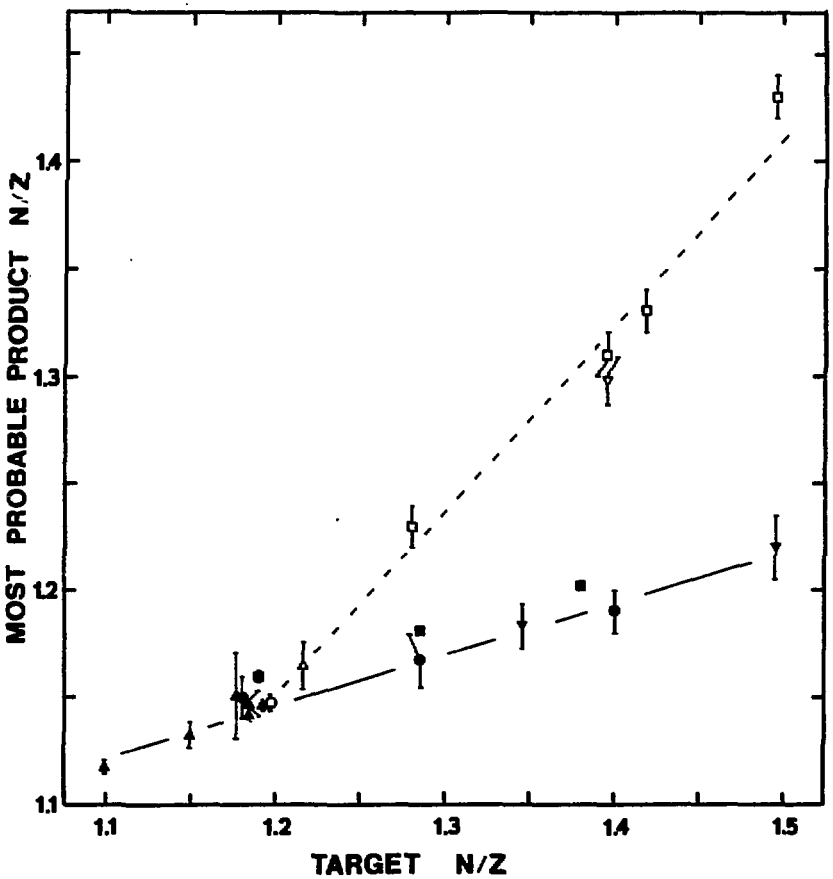

Fig. 5